Journal of Materials Chemistry A

Amphipathic Emulsion Binder for Enhanced Performance of Lithium-Sulfur Batteries

Journal:	*Journal of Materials Chemistry A*
Manuscript ID	TA-ART-02-2024-001037.R1
Article Type:	Paper
Date Submitted by the Author:	14-Apr-2024
Complete List of Authors:	He, Yuan; Anhui University of Technology Jing, Xulong; Anhui University of Technology Lai, Tianxing; The University of Texas at Austin Jiang, Dong; National Institute for Materials Science Wan, Chao; Zhejiang University, Postnikov, Pavel; Tomsk Polytechnic University, Research School of Chemistry & Applied Biomedical Sciences; Vysoka skola chemicko-technologicka v Praze, Guselnikova, Olga; Tomsk Polytechnic University, ; Centre of Excellence for electrochemical surface Technology, Xu, Lixin; Anhui University of Technology, College of Chemistry and Chemical Engineering He, Xiaojun; Anhui University of Technology, Yamauchi , Yusuke; JST-ERATO Yamauchi Materials Space-Tectonics Project, Kagami Memorial Research Institute for Science and Technology, Waseda University, 2-8-26 Nishi-Waseda, Shinjuku, Tokyo 169-0051, Japan Jin, Biyu; The university of Texas at Austin,

Journal of Materials Chemistry A

ARTICLE

Amphipathic Emulsion Binder for Enhanced Performance of Lithium-Sulfur Batteries

Received 00th January 20xx,
Accepted 00th January 20xx

DOI: 10.1039/x0xx00000x

Yuan He, [a] Xulong Jing, [a] Tianxing Lai, [b] Dong Jiang, [c] Chao Wan, *[a,d] Pavel S. Postnikov,[e] Olga Guselnikova, [e] Lixin Xu, [a] Xiaojun He, *[a] Yusuke Yamauchi [f,g,h] and Biyu Jin *[a]

The application of polyvinylidene fluoride (PVDF) binder in lithium-sulfur batteries faces challenges due to inadequate adhesion, undesirable conductivities, limited lithium polysulfides absorbability, and its dependence on the use of toxic N-methyl-2-pyrrolidone solvent. Here, a polysaccharide emulsion binder (HBEA) is synthesized by polymerizing and grafting hydrophilic lithiated acrylic acid, 2-hydroxyethyl acrylate, and hydrophobic butyl acrylate onto the backbone of sodium hyaluronate. The amphipathic nature of the synthesized binder enables outstanding affinity to electrode materials, ensuring exceptional adhesion compared to PVDF in various destructive tests. Additionally, the abundant polar groups in HBEA facilitate effective absorption of lithium polysulfides, leading to enhanced sulfur utilization and improved protection of the lithium anode. Furthermore, the presence of lithiated acrylic acid in HBEA leads to a Li^+ diffusion coefficient 0.6~1 times larger than that of PVDF in the HBEA binder-based cells. As a result, the high-loading HBEA cell (5 mg cm^{-2}) demonstrates an initial discharge capacity of 3.3 mAh cm^{-2} at 0.5C and maintains an 87.8% capacity retention after 75 cycles. This work offers an environmentally friendly and easily producible emulsion binder for high-mass-loading sulfur cathodes.

1. Introduction

The surging demand for electric vehicles in contemporary society has prompted the need for energy storage devices with high energy density. In this regard, lithium-sulfur batteries (LSBs) have emerged as a promising candidate for the next generation of batteries owing to their high theoretical discharge capacity of 1672 mAh g^{-1}.[1-4] However, there are several challenges that currently hinder their practical viability.[5] Specifically, the shuttling of electrolyte-soluble long-chain lithium polysulfides (LiPS) results in low utilization of active sulfur and rapid capacity decay.[6-8] This phenomenon occurs due to the diffusion of the LiPS from the cathode to the anode, leading to the loss of active sulfur in the cathode and a subsequent reduction in battery capacity.[9-11] Moreover, the insulating nature of sulfur leads to the sluggish redox reaction, especially at high current densities, impeding the transport of electrons and ions within the cathodes.[12-14] Furthermore, the significant volume change (~76%) that occurs during the conversion of sulfur to lithium sulfide brings about severe electrode cracking, leading to poor battery cycle life.[15-18]To mitigate the aforementioned issues, researchers have developed various strategies in terms of separators, carbon hosts, catalysts, and binders.[19-24]

Polyvinylidene fluoride (PVDF), a synthetic polymeric binder, is commonly used in lithium-sulfur batteries due to its good chemical and thermal stability as well as its excellent ability to bind conductive materials such as carbon black and super P *via* hydrophobic interactions.[25,26] However, despite its advantages, PVDF still presents several disadvantages: i) poor adhesion with active materials (S/Li_2S), which can lead to the detachment of the active material from the current collector during cycling;[27,28] ii) toxicity and the high price of N-methyl-2-pyrrolidone (NMP) solvent, which can increase the cost and environmental impact of battery production.[29,30] In addition, the high boiling point and low volatility of NMP result in residual solvent content in the final product. This residual NMP can negatively impact the performance of the battery, such as reducing the capacity and increasing the internal resistance;[31-33] iii) poor ionic and electronic conductivities of PVDF, which hinder the transport of lithium ions (Li^+) and electrons within the electrode and limit the overall performances of the batteries;[34,35] iv) weak chemical interactions between PVDF and LiPS, which indicates the incapability of PVDF in

[a] College of Chemistry and Chemical Engineering, Anhui University of Technology, Maanshan, 243002, China. E-mail: wanchao@zju.edu.cn (C. Wan); xjhe@ahut.edu.cn (X. He); biyu.jin@austin.utexas.edu (B. Jin)
[b] Materials Science & Engineering Program and Texas Materials Institute, The University of Texas at Austin, Austin, TX, 78721 USA
[c] Department of Life Science & Medical Bioscience, School of Advanced Science and Engineering, Waseda University, 2-2 Wakamatsu-cho, Shinjuku, Tokyo 162-8480 Japan
[d] College of Chemical and Biological Engineering, Zhejiang University, Hangzhou, 310058, China.
[e] Research School of Chemistry and Applied Biomedical Sciences, Tomsk Polytechnic University, Tomsk, Russian Federation
[f] Australian Institute for Bioengineering and Nanotechnology (AIBN), The University of Queensland, Brisbane, Queensland 4072, Australia
[g] Department of Materials Process Engineering, Graduate School of Engineering, Nagoya University, Nagoya 464-8603, Japan
[h] Department of Chemical and Biomolecular Engineering, Yonsei University, Seoul 03722, South Korea

Electronic Supplementary Information (ESI) available: [details of any supplementary information available should be included here]. See DOI: 10.1039/x0xx00000x

suppressing shuttling effect.[36-38] Those issues have prompted the exploration of alternative binders, with biomass binders being the most attractive category due to their functional groups such as hydroxyl, carboxyl, and amino groups.[39-41] While water-soluble binders derived form biomass can form effective bonding interactions with active materials and current collectors through the these functional groups.[42-44] However, the weak interaction between the hydrophilic binder and hydrophobic conductive materials still impedes their application.[45] The use of carboxymethyl cellulose-styrene butadiene rubber emulsion (CMC-SBR) binder gives us inspiration. The hydrophilic CMC enables good contact with the active materials and current collectors, while the hydrophobic SBR emulsion can closely contact with the conductive additives.[46,47]

In this work, we designed and synthesized a polysaccharide emulsion binder with eco-friendly sodium hyaluronate (HA) as the raw material. Its abundant hydroxyl, amide, and sodium carboxylate groups make it highly capable of adsorbing polysulfides and readily amenable to chemical modification for creating multifunctional binders.[48] Functional monomers including hydrophilic lithiated acrylic acid, 2-hydroxyethyl acrylate, and hydrophobic butyl acrylate were polymerized and grafted on the side chains of acyloxy modified sodium hyaluronate. To assess the performances of the polysaccharide emulsion binder, cycling tests were conducted on sulfur cathodes with low (1 mg cm^{-2}) and high loading (5 mg cm^{-2}). The amphipathicity of the binder enables adequate contact between both hydrophilic and hydrophobic materials in sulfur cathodes, which is characterized by peeling, folding and electrolyte immersing tests. Additionally, the outstanding LiPS absorbability of the as-synthesized polysaccharide emulsion binders was elucidated by theoretical simulation, electrochemical impedance spectroscopy (EIS), and energy dispersive spectroscopy (EDS).[49,50] Moreover, enhanced Li^+ ion transportation was demonstrated by cyclic voltammetry (CV).[42,51] Through various characterizations and analyses, the impact of the emulsion binder on enhanced cell performances is disclosed.

2. Experimental

2.1 Materials

Sodium hyaluronate (HA, M_w = 210 kDa) was purchased from Shandong Freida. Acrylic acid (AA), methacrylic anhydride (MA), butyl acrylate (BA), 2-hydroxyethyl acrylate (HEA), dodecylbenzene sulfonic acid (SDS) and OP-10 were purchased from Macklin. Ammonium persulfate (APS) and sodium hydroxide (NaOH) were purchased from Sinopharm Chemical Reagent. N-methylpyrrolidone (NMP) and sublimed sulfur (S, 99.95%) were purchased from Aladdin. Super P was obtained from Timcal (Switzerland). Ketjen black (KB) was purchased from Suzhou Jilong Energy Technology Co., Ltd. The pH of AA-containing solution was adjusted by lithium hydroxide (LiOH) to 4.5 before use.

2.2 Synthesis of HBEA binders

Firstly, HA (0.5 g) was dissolved in deionized water (50 g). MA (0.00734 g, HA and MA molar ratio: 1:20) was then added dropwise, and the pH was maintained between 7.5 and 8.5. After 24 h of reaction at 3°C, the obtained product was lyophilized, freeze dried, and denoted as HAMA. Secondly, HEA (0.5 g), BA (1.5 g), lithiated AA (3 g), OP-10 (0.04 g), SDS (0.06 g), HAMA (0.5 g) and APS (0.0825 g) were dissolved in deionized water (36 g) and reacted at 70°C for 12 h under argon protection. The obtained emulsion was directly used as binder and denoted as HBEA.

2.3 Preparation of electrodes

To prepare the sulfur cathodes, the sublimated sulfur and the conductive agent (KB) were mixed evenly at a ratio of 9:1, heated at 155°C for 12 h to obtain the S/KB composite. Then, the slurry containing S/KB composite, Super P and binder (HBEA or PVDF) with a mass ratio of 8:1:1 was casted on the carbon-coated aluminum foil and dried at 60°C under vacuum for 12 h. Then, the electrode was punched into 12 mm diameter round discs for use. Each cathode contains 1.2~1.3 mg sulfur per cm^2. To prepare high active material loading electrodes, nickel foam was used as current collector. Each electrode contains 5 mg sulfur per cm^2.

2.4 Characterizations

Fourier transform infrared (FTIR-850) was used to analyze the chemical structure of HBEA polymers. Field emission scanning electron microscope (SEM, Nano SEM430) was used to observe the surface morphologies of the sulfur cathodes and lithium anodes. The elemental compositions of sulfur cathodes were analyzed by X-ray photoelectron spectroscopy (XPS, Thermo Scientific, USA) using Al X-ray source. ^1H nuclear magnetic resonance (NMR) spectra measurement was recorded on Mercury VX- 300 spectrometer. 180◦ peeling tests were performed by a Zwick/Roell Z020 universal material tester.

2.5 In suit UV-Visible Spectra

Sulfur powder (S) and lithium sulfide (Li_2S) were added to a solution of 1,2-dimethoxyethane (DME) and 1,3-dioxolane (DOL) 1:1 by molar ratio of 5:1, and reacted at 70℃ for 24 h to obtain much LiPS solution (average molecular formula Li_2S_6). Then, the binder and Super P of the same quality were weighed and placed in the colorimetric dish, and the LiPS solution was added. After the glove box was sealed, the spectrum of the sample was detected continuously for 12 hours by SHIMADZU UV-2550 UV-visible absorption spectrometer, and the UV-Vis spectrum of 350-550 nm was obtained.

2.6 Electrochemical measurements

The galvanostatic charge-discharge cycling tests were performed on Neware (CT-4008) battery testers in a voltage range of 1.7~2.8 V for half-cells. The CR2025 coin cells were assembled in the Ar-filled glove box. Celgard 2400 was used as separator. The electrolyte used for half cells is composed of 1 M LiTFSI in the mixture of 1,3-Dioxolane (DOL) and 1,2-Dimethoxyethane (DME) (1:1, v/v) with 1% lithium nitrate ($LiNO_3$) as additive. For the electrochemical cycle performance of the low-load sulfur cathode, the 0.5C battery is activated by 0.3C on the first cycle, the 0.3C battery is activated by 0.1C on the first cycle and the 1C battery is activated by 0.3C on the first cycle. In addition, the cycle performance of the high-load sulfur cathode, the first three cycles of the 0.5C battery are activated with 0.3C. EIS and CV tests were conducted on a CHI760E electrochemical workstation. CV was performed in a voltage range of 1.7~2.8 V with different scanning rates of 0.005, 0.10, 0.15, 0.2, and 0.25 mV s^{-1}. The diffusion coefficients of Li^+ are calculated using the classical Randles–Sevcik equation:

$$I_p = (2.69\times10^5)\, n^{1.5} A D_{Li^+}^{0.5} v^{0.5} C_{Li^+}$$

Wherein, Ip indicates the peak current, C_{Li^+} is the Li-ion concentration in the electrolyte, A is the electrode area, v is the scanning rate (V s^{-1}), n is the number of electrons in the reaction (S=2), and D_{Li^+} is the Li-ion diffusion coefficient (cm^2 s^{-1}). EIS was recorded at open circuit voltage in the frequency range of 1 MHz to 1 Hz with an AC voltage amplitude of 10 mV. All the tests were performed at room temperature.

2.7 Theoretical simulation

The binding energies between the binders and polysulfides were simulated using the Vienna ab initio simulation package (VASP). Generalized gradient approximation (GGA) with Perdew-Burke-Ernzerhof (PBE) exchange-correlation functional was employed along with the projector augmented wave (PAW) pseudopotentials. An energy cutoff of 550 eV and a 1 × 1 × 1 Γ-centered k-point mesh were utilized. The structures of the HBEA and PVDF were simplified (**Figure S1**). Li_2S_6 was selected to represent polysulfides. Simplified HBEA, PVDF, and Li_2S_6 molecules were relaxed individually before being combined and relaxed together. The binding energies were calculated based on the following equation: $E_{binding} = E_{binder+Li2S6} - E_{binder} - E_{Li2S6}$.

3. Results and discussion

3.1 Structure of HBEA emulsion binder

The HBEA emulsion binder was synthesized through a radical polymerization process (**Figures 1a** and **S2**). Initially, acyloxy groups were grafted onto the backbone of HA *via* an esterification reaction with carboxyl groups. This step introduced reactive C=C groups, which played a crucial role in the subsequent polymerization. Then, three functional monomers were introduced: i) hydrophilic lithiated AA and HEA, which could facilitate hydrogen bonding with the active collector.[52,53] Lithiated AA was reported to facilitate the transport of Li^+ due to its carboxylic acid groups during the peristaltic movement of the polymer binder. ii) Hydrophobic BA, which showed a strong affinity for conductive materials and possesses a low glass transition temperature to enhance the flexibility of the binder (**Figure 1b**) .

Fourier transform infrared (FTIR) spectroscopy was applied to characterize the successful preparation of HBEA, as shown in **Figure 1c**. The stretching vibration peaks of -OH, C-H, N-H, -COO-, and C-N groups in HBEA backbone or side-chains appear at 3423 cm^{-1}, 2922 cm^{-1}, 1558 cm^{-1}, 1409 cm^{-1}, and 1156 cm^{-1}, respectively. Furthermore, a comparison of the peak positions of C=O in HA and HBEA reveals a shift from the initial 1617 cm^{-1} to 1717 cm^{-1}, indicating the formation of ester groups after the reaction of HA and MA.[54,55] More importantly, the disappearance of C=C groups (1680~1620 cm^{-1}) indicates the complete polymerization of reactive C=C groups on the backbone of HA. The successful synthesis of HA, HAMA and HBEA was further confirmed by NMR analysis (**Figure S3**). The emergence of new proton peaks at 6.16/5.73 ppm and 1.93 ppm, attributed to the vinyl groups and methyl peaks, respectively, observed in the ^1H NMR spectrum of HAMA, can be attributed to the modification of the methacrylate group in the HA backbone.[56] Additionally, in the ^1H NMR spectrum of the final product HBEA, the protons from vinyl groups disappear, while the signals at 0.92 ppm, 4.16 ppm, and 3.81 ppm, attributed to the methyl and ethyl groups from the introduced polyHEA and polybag, become more prominent.

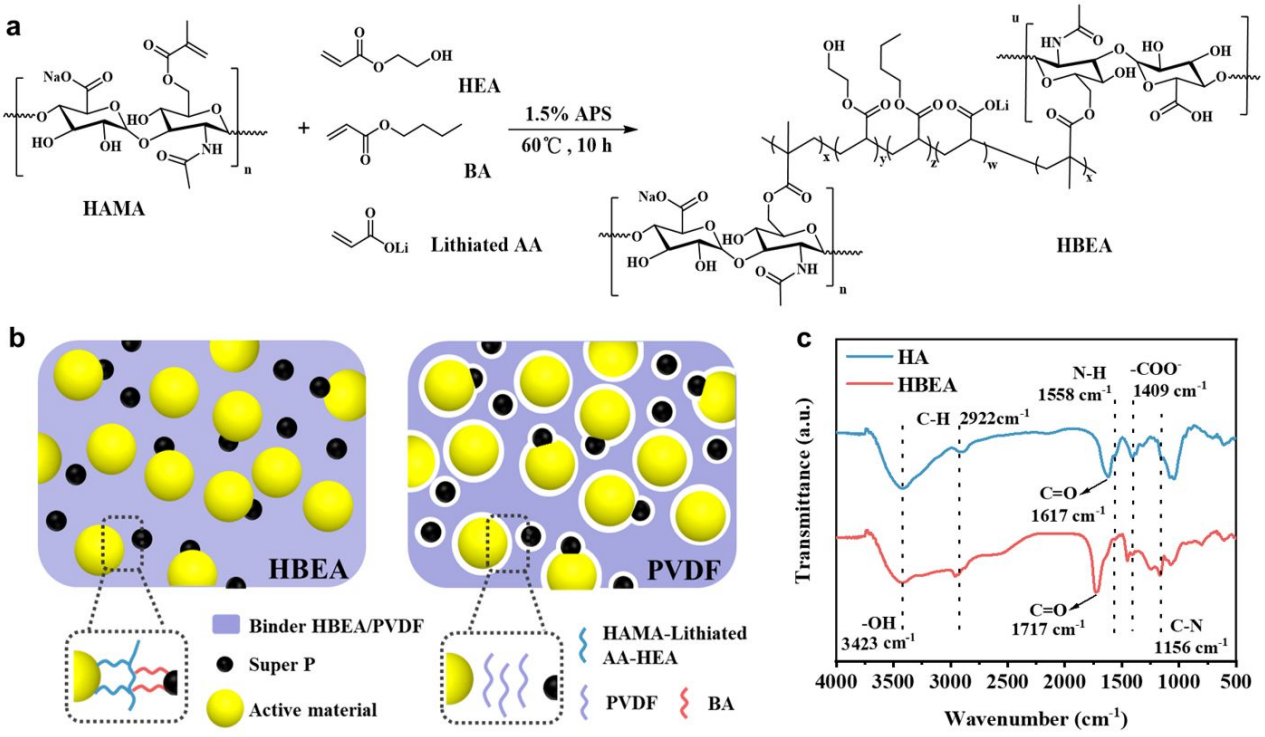

Figure 1. (a) Synthesis process of HBEA binder, (b) Schematic illustration of the interactions between binder (HBEA or PVDF) and electrode materials, (c) FTIR of HA and HBEA binder.

3.2 Adhesive properties of HBEA binder

The cohesion between the polymer binder and electrode particles, as well as its connection to the current collector, plays a vital role in maintaining the structural integrity of cathodes. This, in turn, leads to enhanced capacity retention.[57] To comprehensively showcase the adhesive properties of the synthesized HBEA binder, a series of tests were performed, including folding assessments, tape peeling evaluations, and electrolyte immersing examinations. As shown in **Figures 2a**, **b**, after folding and unfolding the cathode discs three times, the electrode particles located at the creases become detached from the PVDF-based cathode, revealing the underneath aluminum foil. In contrast, the HBEA binder demonstrates a notable ability to securely affix the particles onto the aluminum surface. Subsequent tape peeling tests (**Figure 2c**) unveil minimal particle detachment from the S/HBEA electrode, while the tape peeled from the S/PVDF electrode exhibits a darkened appearance, reaffirming inadequate adhesion of PVDF. As shown in the **Figure S4**, the average peeling force of HBEA electrode is 2.80 N, which is about 2.1 times higher than that of PVDF (1.35 N).

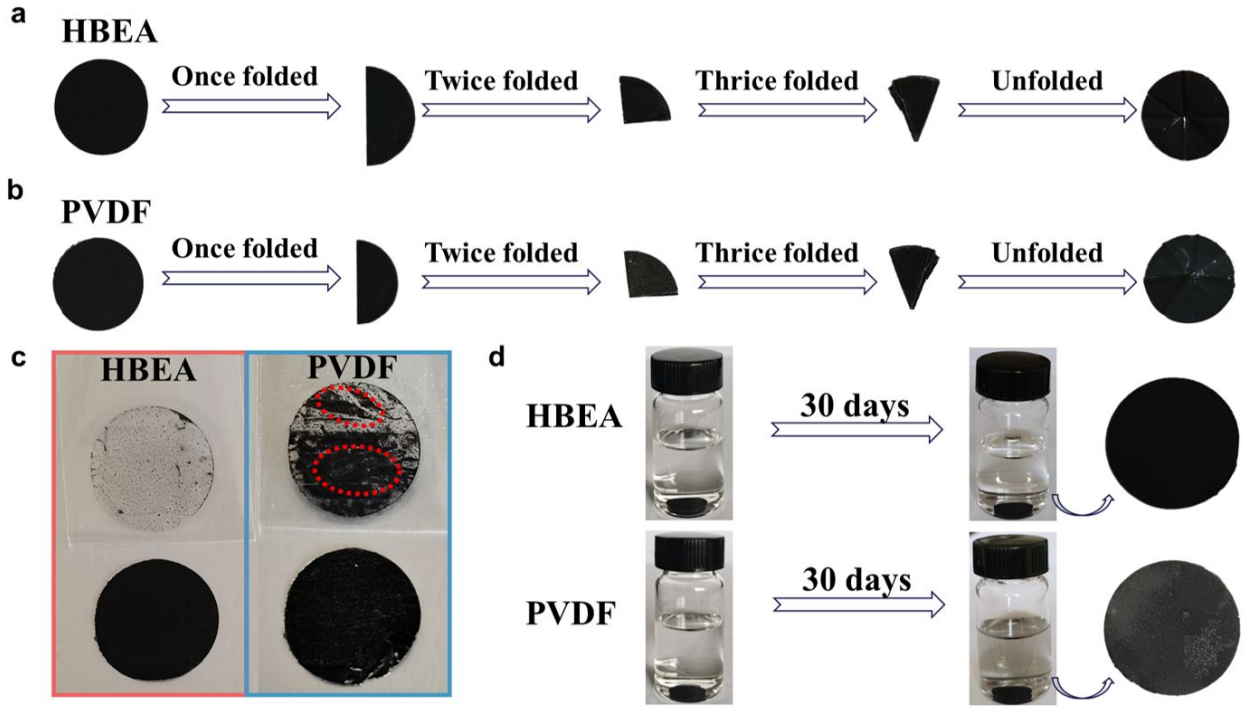

Figure 2. Folding tests of (a) HBEA- and (b) PVDF-based sulfur cathodes. (c) Tape peeling tests. (d) Electrolyte immersing tests (30 days at room temperature).

Notably, the adhesive properties of the binder in the electrolyte medium are generally inferior to those in air because electrolyte can easily penetrate into the interfaces among particles, binder and current collector. Therefore, it becomes imperative to access the adhesion of the as-synthesized binder in electrolyte. As shown in **Figure 2d**, after immersing the S/HBEA and S/PVDF electrodes in DME/DOL mixture for 30 days at room temperature, a notable contrast emerges: the S/PVDF-containing vial exhibits a darkened hue, while the S/HBEA-containing vial remains visibly clear. Meanwhile, due to extensive particle detachment from the S/PVDF electrode, the surface of the S/PVDF electrode displays a speckled appearance with a loosely structured morphology, which can be clearly seen in the photograph.

3.3 Electrochemical performance

The influence of the synthesized emulsion binder on electrochemical performances was evaluated in coin cells with conventional PVDF binder as a reference. In **Figure 3a**, it is evident that the S/HBEA cell outperforms S/PVDF with a notably higher average discharge capacity of 682.89 mAh g^{-1} at 0.3C. In addition, the capacity retention of S/HBEA is as high as 85.2% after 100 cycles (calculated based on the 2nd cycle), which is 1.2 times higher than that of S/PVDF. Figure 3b illustrates the cyclability of different binder-based S cathodes at a more challenging 0.5C. After the formation cycle, the S/HBEA cell can deliver an initial discharge capacity of 866.13 mAh g^{-1} with 62.44% capacity retention after 300 cycles. Conversely, S/PVDF merely achieves an initial discharge capacity of 652.87 mAh g^{-1} with 54.69% capacity retention under identical testing conditions. Even at a higher current density of 1C, S/HBEA exhibits superior cyclability during 300 cycles with a capacity retention of 84.6%, nearly 10% higher than that of S/PVDF (calculated based on the 4th cycle, **Figure 3c**). Notably, both S/HBEA and S/PVDF experience a rapid capacity decay during the initial 10 cycles, accounting for an 82.5% and 62.7% of the total capacity fade, respectively (**Figure S5**). Subsequently, S/HBEA maintains an impressively high-capacity retention of 84.7%, 1.4-fold higher than that of S/PVDF.

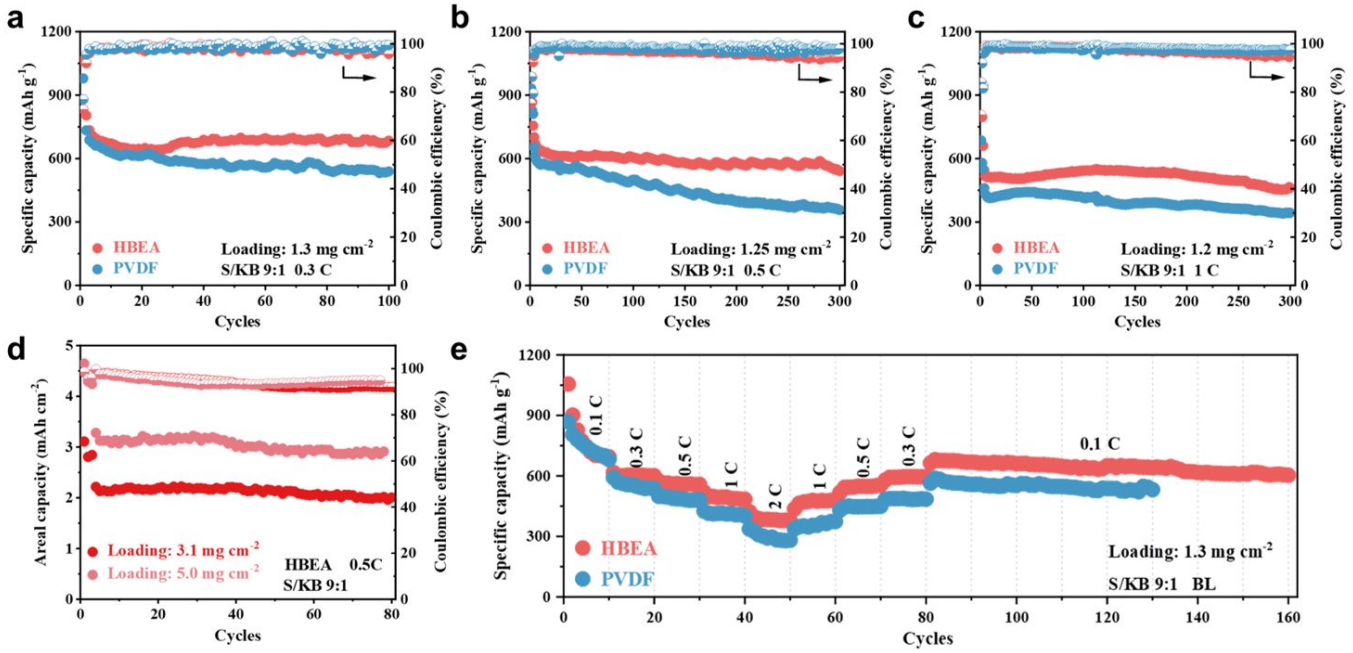

Figure 3. Electrochemical performances of different binder-based sulfur cathodes. Cycling performance and Coulombic efficiency of S/HBEA and S/PVDF at (a) 0.3C, (b) 0.5C and (c) 1C. (d) Cycling performances and Coulombic efficiency of high mass loading S/HBEA. (e) Rate performances of S/HBEA and S/PVDF.

Although the specific discharge capacity of lithium-sulfur batteries is several times higher than traditional lithium-ion batteries, the average operation voltage of LSBs is low (2.1 V *vs.* 3.5 V).[58] Therefore, to demonstrate the competitiveness of lithium-sulfur batteries (LSBs), it becomes imperative to employ high-mass-loading sulfur (3~7 mg cm^{-2}). We prepared sulfur cathodes with mass loading of 3.1 and 5.0 mg cm^{-2}. These cathodes were subjected to cycling at 0.5 C (**Figures 3d** and **S6**). After three formation cycles at 0.1C, these cells deliver initial discharge capacities of 713.97 mAh g^{-1} (2.2 mAh cm^{-2}) and 655.85 mAh g^{-1} (3.3 mAh cm^{-2}). Impressively, these capacities remain consistent, registering at 650.03 mAh g^{-1} (2.0 mAh cm^{-2}) and 572.17 mAh g^{-1} (2.9 mAh cm^{-2}) after 75 cycles at 0.5C, corresponding to the capacity retention of 91.5% and 87.8% (calculated based on the 4th cycle). It is noted that the cycling performances of both high loading cells remain nearly identical throughout the cycling process, indicating the uniform thick electrode helped with HBEA binder.

In addition to the enhanced capacity retention, the introduction of HBEA also leads to improved redox kinetics at high operating current (**Figures 3e** and **S7**). Specifically, S/HBEA delivers reversible discharge capacities of 781, 603, 561, 493, and 387 mAh g^{-1} at 0.1, 0.3, 0.5, 1, and 2C. When the current density returns to 0.1C, S/HBEA still can achieve 602 mAh g^{-1} after 80 cycles, corresponding to the 86.8% capacity retention benchmarked against the 10th cycle. Significantly, while the S/PVDF cell exhibits marginally lower discharge capacities compared to S/HBEA, it falls short of delivering satisfactory performance at 2C. Moreover, as the current rates are gradually reduced, the capacity disparity between the S/HBEA and S/PVDF cells becomes more pronounced, suggesting a higher loss of active materials in the S/PVDF cell.

To figure out the reasons for the evidently enhanced cycling and rate performances of HBEA-based cells, various characterizations were conducted to the cycled cells. As shown in the impedance spectroscopy (**Figure S8a**), prior to cycling, the S/HBEA cell demonstrates lower resistance (70.04 Ω) compared to the S/PVDF cell (103.81 Ω), a discrepancy attributed to the presence of lithiated polyacrylic acid within HBEA, which imparts Li^+ conductivity. After 100 and 150 cycles (**Figures S8b**, **c**), the resistances of both S/HBEA and S/PVDF cells obviously decrease to ~20 Ω and ~30 Ω, respectively, which would be the result of solid-liquid conversion reactions. However, with an extension of cycling to 250 cycles (**Figure S8d**), the resistance of the S/PVDF cell experiences an increase (35.56 Ω), concurrently accompanied by the emergence of the secondary semicircle, corroborating earlier findings. The resistance contributions originating from the bulk materials and electrode-electrolyte interfaces are represented by the semicircle at high frequency region. The second semicircle at medium-to low frequency stands for the charge-transfer resistance, which is mainly determined by the anode-electrolyte interface.[59] It is reported that the deposition of LiPS on the lithium surface would result in the formation of an insulating sulfur-rich layer. Therefore, a deficiency in effective adsorption of lithium polysulfides would result in a considerable increase in charge-transfer resistance after cycling.

3.4 Adsorbability of binders to polysulfide lithium

To assess the LiPS adsorbability of binder, static adsorption experiments and in-situ UV-vis spectroscopy were employed. As shown in **Figure 4a**, the solution in HBEA-containing vial became lighter after 4 h, at the same time, the white binder powder transforms to a yellow hue due to adsorbing LiPS. It is reported that polar groups such as amide, carboxylic acid, ester, and hydroxy groups exhibit a strong affinity for LiPS, which are massively present in the backbone and side chains of the HBEA binder.[60] However,

fluorine groups in PVDF displays weak binding energy to LiPS, with which the yellow color shows minimal change. Moreover, the efficacy of the HBEA binder in adsorbing LiPS is further demonstrated by in situ UV-vis spectroscopy (**Figures 4b**, **c**), wherein a discernible Li_2S_6 peak within 360 to 450 nm region is evident. After exposure to HBEA-super P composite, the strong Li_2S_6 peak gradually diminishes, while the deep red-orange solution becomes light yellow. Such pronounced adsorption capability of the HBEA binder is further confirmed by theoretical calculations (**Figure 4e**). Binding energies of the O sites in HBEA are 1~2 times higher than that of the F site in PVDF. In other words, compared with the PVDF control, the HBEA binder can effectively sequester soluble polysulfides generated during cycling within the cathode side, thereby greatly improve the cycling stability(**Figure 4d**).

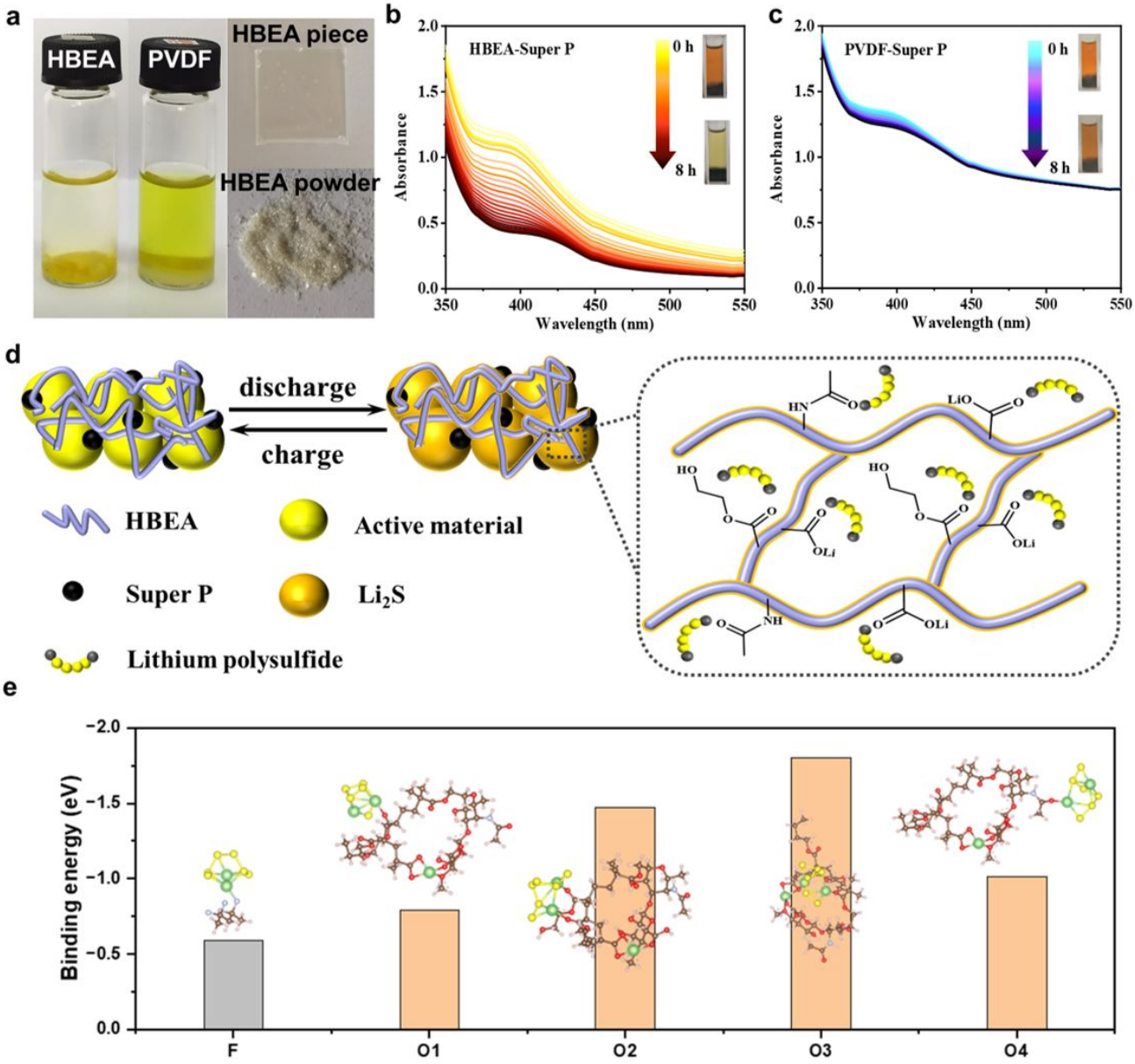

Figure 4. (a) LiPS adsorbability of dried HBEA and PVDF binder. In-situ UV-vis spectra of Li_2S_6 solution containing, (b) HBEA-Super P or (c) PVDF-Super P composites, (d) Illustration of the interactions of HBEA to LiPS, (e) Calculated binding energies of polymer fragments to Li_2S_6.

Post-mortem analysis including SEM, EDS, and XPS of the cycled coin cells were conducted to cross-validated the functionality of the HBEA binder. **Figures 5a, b, S9** and **S10** depict the SEM images of the cycled S/HBEA and S/PVDF cathodes, respectively. Due to the crosslinked structure of HBEA binder, the structural integrity of S/HBEA cathode (discharge state) is well-preserved comparing with S/PVDF. Evidently, there are some large protuberances and wide cracks appear on the surface of S/PVDF, which would be resulted from the structure limitations of linear PVDF in interacting with LiPS. Without an effective binder, the nucleation kinetics would be hindered and the generated S is likely to lack adequate contact with conductive agent and form “dead” S. The protuberances in **Figure 5b** could be the evidence for the formation of “dead” S on the S/PVDF surface, manifesting as more prominent white regions due to reduced

conductivity. The relatively higher atomic concentration of S element in the surface of Li anode (paired with S/PVDF cathode) further reveal the more severe cathode-to-anode crossover caused by LiPS shuttling (**Figures 5c, d**). Notably, we observe a distinct pair of characteristic peaks in the vicinity of ~167.0 eV within both S 2p XPS spectra (**Figures 5e, f**). These peaks can be attributed to the presence of electrochemically irreversible compounds known as thiosulfate. Fortunately, polysulfides have the capability to interconnect with detrimental thiosulfates. This interaction involves the insertion of S–S bonds to form polythionate complexes and lower-ordered polysulfides, effectively immobilizing sulfur and augmenting sulfur utilization. The surface of Li anode (paired with S/PVDF cathode) exhibits a significantly stronger thiosulfate intensity compared to that paired with S/HBEA, implying an extremely uncontrollable sulfur conversion. [61,62]

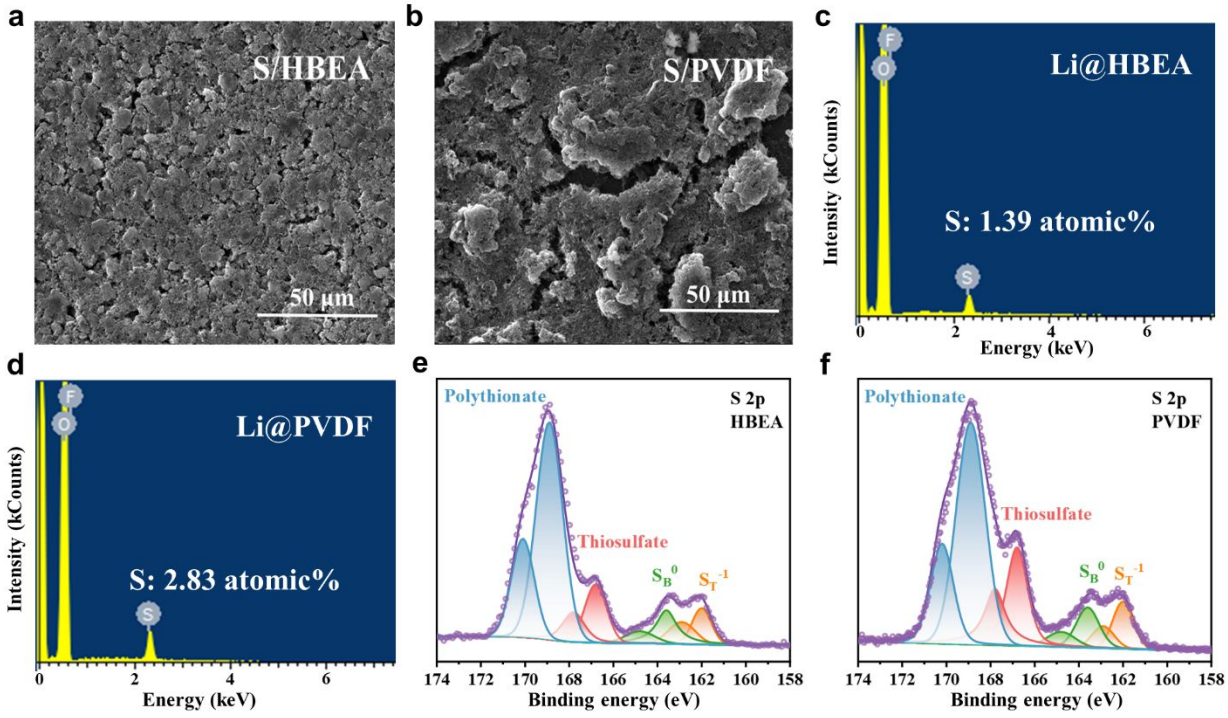

Figure 5. SEM images of cycled (a) S/HBEA and (b) S/PVDF cathodes. EDS of cycled lithium anodes paired with (c) HBEA-based and (d) PVDF-based sulfur cathodes. XPS S 2p region for (e) S/HBEA (f) S/PVDF cathodes after cycling.

3.5 Lithium-ion diffusion coefficient of sulfur cathodes

Apart from the remarkable LiPS absorbability of HBEA binder, we also noticed enhanced cyclability of S/HBEA at higher current density, indicating improved redox kinetic within the S/HBEA cell. CV measurements are conducted to validate this observation. **Figures 6a**, **b** exhibit the CV plots of S/HBEA and S/PVDF cells for successive five cycles at gradually increased current densities. S/HBEA demonstrates evidently heightened response currents at both cathodic and anodic scans and smaller polarization compared to those of S/PVDF, indicating a greater quantity of sulfur and lithium sulfides partake in the redox reactions in S/HBEA.[63,64] In addition, by plotting the oxidation and reduction (**Figures 6c**, **d**) CV peak currents (Ip) versus square root of scan rates ($V^{0.5}$), the lithium-ion diffusion coefficients of different binder-based cells can be compared, which is proportional to the slope of Ip-$V^{0.5}$ curves. Apparently, the slopes of Ip-$V^{0.5}$ curves for S/HBEA cell consistently surpass those of the S/PVDF cell throughout the entire redox process.[65] The subsequent calculation revealing that the Li^+ ions coefficients of S/HBEA are 1.6~2 times of S/PVDF (**Table S1**). This disparity can be attributed to the presence of lithiated polyacrylic acid component in the HBEA binder, where Li^+ can be transferred to carboxyl acid groups via the peristaltic motion of HBEA.

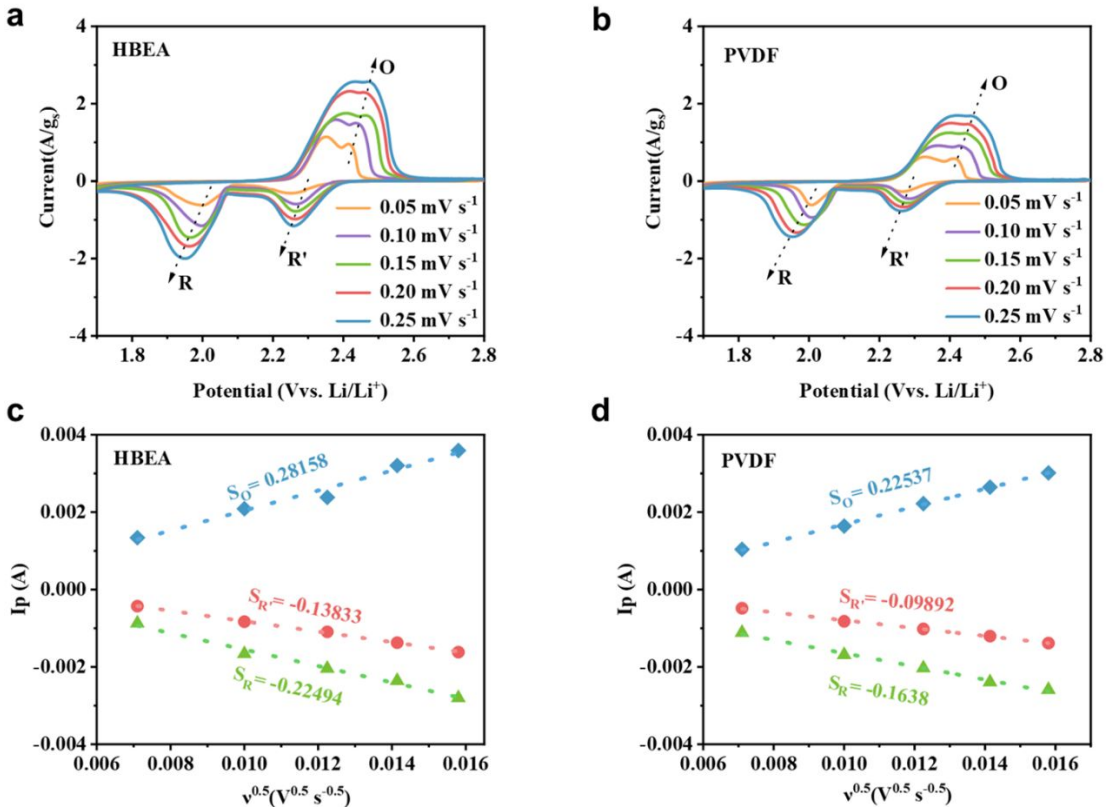

Figure 6. CV plots of (a) S/HBEA and (b) S/PVDF cells with the scan rates of 0.05, 0.1, 0.15, 0.2, and 0.25 mV s^{-1}. Plots of (c) S/HBEA and (d) S/PVDF oxidation and reduction CV peak currents versus square root of scan rates.

4. Conclusions

In summary, we have presented a polysaccharide emulsion binder with a rich array of polar groups, hydrophobic and hydrophilic components, as well as Li^+ conductive species. As the result of these attributes, the synthesized binder demonstrates outstanding LiPS absorbability and superior adhesion. Furthermore, the Li^+ diffusion coefficients within the emulsion binder-based cell also demonstrate 0.6~1 times increase in comparison to cells utilizing PVDF binder. Notably, the S/HBEA cell achieves an initial discharge capacity of 866.13 mAh g^{-1} at 0.5C with a capacity decay of merely 0.13% per cycle during 300 cycles. The S/HBEA cell with high mass loading (5 mg cm^{-2}) delivers an initial discharge capacity of 3.3 mAh cm^{-2} at 0.5C, which can be maintained at 87.8% during 75 cycles. The evident enhancements in electrochemical performance, coupled with the straightforward emulsion polymerization technique, underscore the promising potential of the designed emulsion binder. By seamlessly integrating this functional binder with cutting-edge sulfur cathodes and advanced electrolytes, we anticipate a substantial augmentation in the operational lifespan of practical lithium-sulfur cells.

Author Contributions

Yuan He: Investigation, Data curation, Methodology, Visualization, Writing - reiew & editing. Xulong Jing: Investigation, Data curation, Visualization. Dong Jiang, Lixin Xu: Resources, Supervision. Chao Wan, Pavel S. Postnikov, Olga Guselnikova, Xiaojun He and Yusuke Yamauchi: Resources, Writing - review & editing. Tianxing Lai: Computational analysis. Biyu Jin : Conceptualization, Funding acquisition, Resources, Writing - Original Draft, Writing - review & editing.

Conflicts of interest

There are no conflicts to declare.

Acknowledgements

This work is supported by the National Natural Science Foundation of China (No. 22108002 and 22108238) and the China Postdoctoral Science Foundation (2019M662060, 2020T130580, PC2022046). Additionally, this work is also supported by the JST-ERATO Yamauchi Materials Space Tectonics Project (JPMJER2003) and the UQ-Yonsei International Joint Research Project. This work was performed in part at the Queensland node of the Australian National Fabrication Facility, a company established under the National Collaborative Research Infrastructure Strategy to provide nano and microfabrication facilities for Australia's researchers. he authors are also grateful to the Shiyanjia Lab (www.shiyanjia.com) for characterizing the materials used in this study. We express our gratitude for English editing software, such as Grammarly and

ChatGPT, for refining language and checking grammatical errors in our manuscript.

Notes and references

1 X. Liang, J. Yun, Y. Wang, H. Xiang, Y. Sun, Y. Feng and Y. Yu, *Nanoscale*, 2019, **11**, 19140-19157.
2 W. Kang, N. Deng, J. Ju, Q. Li, D. Wu, X. Ma, L. Li, M. Naebe and B. Cheng, *Nanoscale*, 2016, **8**, 16541-16588.
3 R. Guo, J. Wang, S. Zhang and W. -Q. Han, *Chem. Eng. J.*, 2020, **388**, 124316.
4 X. Hong, J. Jin, Z. Wen, S. Zhang, Q. Wang, C. Shen and K. Rui, *J. Power Sources*, 2016, **324**, 455-461.
5 C. Wang, Y. Ma, X. Du, H. Zhang, G. Xu and G. Cui, *Battery Energy*, 2022, **1**, 20220010.
6 J. Qiu, S. Wu, Y. Yang, H. Xiao, X. Wei, B. Zhang, K. N. Hui and Z. Lin, *ACS Appl. Mater. Interfaces*, 2021, **13**, 55092-55101.
7 P. Mu, T. Dong, H. Jiang, M. Jiang, Z. Chen, H. Xu, H. Zhang and G. Cui, *Energy Fuels*, 2021, **35**, 1966-1988.
8 P. Mu, C. Sun, C. Gao, L. Li, H. Zhang, J. Li, C. Li, S. Dong and G. Cui, *ACS Energy Lett.*, 2023, **8**, 3733-3741.
9 Q. Shao, S. Zhu and J. Chen, *Nano Res.*, 2023, **16**, 8097-8138.
10 Y. Wang, X. Huang, S. Zhang and Y. Hou, *Small Methods*, 2018, **2**, 1700345.
11 B. Jin, D. Wang, L. Song, Y. Cai, A. Ali, Y. Hou, J. Chen, Q. Zhang and X. Zhan, *Electrochim. Acta*, 2021, **365**, 137359.
12 J. Xie, Y. W. Song, B. Q. Li, H. J. Peng, J. Q. Huang and Q. Zhang, *Angew. Chem. Int. Ed.*, 2020, **59**, 22150-22155.
13 R. Wang, H. Kang and M. J. Park, *ACS Appl. Energy Mater.*, 2021, **4**, 2696-2706.
14 S. Lee, K. Sim, J. Kwon, D. Seok and K. Eom, *Electrochim. Acta*, 2022, **412**, 140092.
15 C. Li, Q. Sun, Q. Zhang, C. Xu, S. Wang, Y. Ma, X. Shi, H. Zhang, D. Song and L. Zhang, *Chem. Eng. J.*, 2023, **455**, 140706.
16 M. Zhang, S. Geng, G. Yan, J. Dong, H. Ji, Y. Feng, X. Hu, B. Liu and X. Zhang, *J. Colloid Interface Sci.*, 2023, **633**, 1-10.
17 P. Mu, S. Zhang, H. Zhang, J. Li, Z. Liu, S. Dong and G. Cui, *Adv. Mater.*, 2023, **35**, 2303312.
18 B. Jin, D. Wang, Y. He, J. Mao, Y. Kang, C. Wan, W. Xia, J. Kim, M. Eguchi and Y. Yamauchi, *Chem. Sci.*, 2023, **14**, 7956-7965.
19 H. Yuan, T. Liu, Y. Liu, J. Nai, Y. Wang, W. Zhang and X. Tao, *Chem. Sci.*, 2019, **10**, 7484-7495.
20 H. Zhao, N. Deng, J. Yan, W. Kang, J. Ju, Y. Ruan, X. Wang, X. Zhuang, Q. Li and B. Cheng, *Chem. Eng. J.*, 2018, **347**, 343-365.
21 Y. Chen, T. Wang, H. Tian, D. Su, Q. Zhang and G. Wang, *Adv. Mater.*, 2021, **33**, 2003666.
22 Z. Wei, Y. Ren, J. Sokolowski, X. Zhu and G. Wu, *Infomat*, 2020, **2**, 483-508.
23 H. Li, J. Lampkin, Y. Chien, L. Furness, D. Brandell, M. J. Lacey and N. Garcia-Araez, *Electrochim. Acta*, 2022, **403**, 139572.
24 Z. Zhou, G. Li, J. Zhang and Y. Zhao, *Adv. Funct. Mater.*, 2021, **31**, 2107136.
25 P. Mu, H. Zhang, H. Jiang, T. Dong, S. Zhang, C. Wang, J. Li, Y. Ma, S. Dong and G. Cui, *J. Am. Chem. Soc.*, 2021, **143**, 18041-18051.
26 D. Chen, M. Song, M. Zhu, T. Zhu, P. Kang, X. Yang and G. Sui, *ACS Appl. Energy Mater.*, 2022, **5**, 5287-5295.
27 H. Wang, D. Wei, J. Zheng, B. Zhang, M. Ling, Y. Hou and C. Liang, *ACS Appl. Energy Mater.*, 2020, **3**, 11893-11899.
28 X. Zhu, W. Jiang, S. Zhao, R. Huang, M. Ling, C. Liang and L. Wang, *Nano Energy*, 2022, **96**, 107093.
29 X. Dong, X. Liu, P. K. Shen and J. Zhu, *Adv. Funct. Mater.*, 2023, **33**, 2210987.
30 B. Jin, D. Wang, J. Zhu, H. Guo, Y. Hou, X. Gao, J. Lu, X. Zhan, X. He and Q. Zhang, *Adv. Funct. Mater.*, 2021, **31**, 2104433.
31 T. Chen, B. Cheng, G. Zhu, R. Chen, Y. Hu, L. Ma, H. Lv, Y. Wang, J. Liang, Z. Tie, Z. Jin and J. Liu, *Nano Lett.*, 2017, **17**, 437-444.
32 M. Tian, J. Zhao, H. Liu, Y. Li, Z. Wan, Z. Li, G. Wu, K. Wang, T. Zhou, Y. Tan, Y. Hou, W. Ni, M. Ling and C. Liang, *Sep. Purif. Technol.*, 2022, **300**, 121684.
33 L. Zhong, Y. Mo, K. Deng, S. Wang, D. Han, S. Ren, M. Xiao and Y. Meng, *ACS Appl. Mater. Interfaces*, 2019, **11**, 28968-28977.
34 J. Liu, Y. Li, Y. Xuan, L. Zhou, D. Wang, Z. Li, H. Lin, S. Tretiak, H. Wang, L. Wang, Z. Guo and S. Zhang, *Acs Appl. Mater. Interfaces*, 2020, **12**, 17592-17601.
35 Z. Zhang, C. Chen, J. Xu, Z. Lin and Z. Lin, *ACS Appl. Energ. Mater.*, 2022, **5**, 4691-4697.
36 H. Yi, T. Lan, Y. Yang, H. Zeng, T. Zhang, T. Tang, C. Wang and Y. Deng, *Energy Storage Mater.*, 2019, **21**, 61-68.
37 X. Wu, C. Luo, L. Du, Y. Xiao, S. Li, J. Wang, C. Wang and Y. Deng, *ACS Sustain. Chem. Eng.*, 2019, **7**, 8413-8418.
38 R. Guo, S. Zhang, J. Wang, H. Ying and W. Han, *ChemSusChem*, 2020, **13**, 819-826.
39 Q. Qi, Y. Deng, S. Gu, M. Gao, J. Hasegawa, G. Zhou, X. Lv, W. Lv and Q. Yang, *ACS Appl. Mater. Interfaces*, 2019, **11**, 47956-47962.
40 X. Dong, Q. Deng, F. Liang, P. K. Shen, J. Zhu and C. Tang, *J. Energy Chem.*, 2023, **86**, 118-134.
41 B. Jin, T. Lai and A. Manthiram, *ACS Energy Lett.*, 2023, **8**, 3767-3774.
42 W. Chen, T. Lei, T. Qian, W. Lv, W. He, C. Wu, X. Liu, J. Liu, B. Chen, C. Yan and J. Xiong, *Adv. Energy Mater.*, 2018, **8**, 1702889.
43 R. Sun, J. Hu, X. Shi, J. Wang, X. Zheng, Y. Zhang, B. Han, K. Xia, Q. Gao, C. Zhou and L. Mai, *Adv. Funct. Mater.*, 2021, **31**, 2104858.
44 Y. Yang, J. Qiu, L. Cai, C. Liu, S. Wu, X. Wei, D. Luo, B. Zhang, X. Yang, K. N. Hui, J. Liu and Z. Lin, *ACS Appl. Mater. Interfaces*, 2021, **13**, 33066-33074.
45 Y. Tan, W. Wang, L. Gao, A. Guan and G. Wang, *Chin. J. Polym. Sci.*, 2023, **41**, 1027-1036.
46 C. Wei and M. N. Obrovac, *J. Electrochem. Soc.*, 2019, **166**, A3217-A3221.
47 B. Jin, L. Yang, J. Zhang, Y. Cai, J. Zhu, J. Lu, Y. Hou, Q. He, H. Xing, X. Zhan, F. Chen and Q. Zhang, *Adv. Energy Mater.*, 2019, **9**, 1902938.
48 J. Liu, Q. Zhang and Y. Sun, *J. Power Sources*, 2018, **396**, 19-32.
49 J. H. Ahn, D. -A. Lim, J. Kim, T. -S. You and D. -W. Kim, *J. Ind. Eng. Chem.*, 2022, **108**, 484-492.
50 H. Wang, V. Sencadas, G. Gao, H. Gao, A. Du, H. Liu and Z. Guo, *Nano Energy*, 2016, **26**, 722-728.
51 P. Han, S. -H. Chung, C. -H. Chang and A. Manthiram, *ACS Appl. Mater. Interfaces*, 2019, **11**, 17393-17399.
52 L. Hu, X. Zhang, P. Zhao, H. Fan, Z. Zhang, J. Deng, G. Ungar and J. Song, *Adv. Mater.*, 2021, **33**, 2104416.
53 B. Jin, Z. Cui and A. Manthiram, *Angew. Chem. Int. Ed.*, 2023, **62**, e202301241.
54 M. -H. Hsiao, K. -H. Lin and D. -M. Liu, *Soft Matter*, 2013, **9**, 2458-2466.
55 Y. Shi, F. Gao, Y. Xie, X. Xu, F. Li, X. Han, X. Yao, D. Wang, Y. Hou, X. Gao, Q. He, J. Lu, X. Zhan and Q. Zhang, *J. Power Sources*, 2023, **580**, 233267.
56 H. Si, T. Xing, Y. Ding, H. Zhang, R. Yin and W. Zhang, *Polymers*, 2019, **11**, 1584.
57 H. Huang, D. Wei, X. Zhu, Z. Wu and M. Ling, *Mater. Chem. Phys.*, 2023, **295**, 127129.

58 B. Jin, Y. Li, J. Qian, X. Zhan and Q. Zhang, *ChemElectroChem*, 2020, **7**, 4158-4176.
59 T. Lai, A. Bhargav and A. Manthiram, *Adv. Funct. Mater.*, 2023, **33,** 2304568.
60 Z. W. Seh, Q. Zhang, W. Li, G. Zheng, H. Yao and Y. Cui, *Chem. Sci.*, 2013, **4**, 3673-3677.
61 Q. Deng, X. Dong, P. K. Shen and J. Zhu, *Adv. Sci.*, 2023, **10**, 2207470.
62 T. Ren, X. Wang, N. Wang, P. K. Shen and J. Zhu, *J. Mater. Chem. A Materials Chemistry A*, 2024, **12**, 5307-5318.
63 Y. -H. Liu, W. Chang, J. Qu, Y. -Q. Sui, Y. Abdelkrim, H. -J. Liu, X. -Z. Zhai, Y. -G. Guo and Z. -Z. Yu, *Energy Storage Mater.*, 2022, **46**, 313-321.
64 J. Liu, Z. Chu, P. Li, J. Lin, Y. Yang and Z. Yang, *Colloids and Surfaces A*, 2023, **670**, 131526.
65 B. Hu, J. Xu, Z. Fan, C. Xu, S. Han, J. Zhang, L. Ma, B. Ding, Z. Zhuang, Q. Kang and X. Zhang, *Adv. Energy Mater.*, 2023, **13**, 2203540.